2D-ERT monitoring of soil moisture seasonal behaviour in a river levee: A case study

Clara Jodry, Sergio Palma Lopes, Yannick Fargier, Martin Sanchez, Philippe Cote

HAL Id: insu-02142990

https://insu.hal.science/insu-02142990

Submitted on 26 Aug 2019

Accepted Manuscript

2D-ERT monitoring of soil moisture seasonal behaviour in a river levee: A case study

Clara Jodry, Sérgio Palma Lopes, Yannick Fargier, Martin Sanchez, Philippe Côte
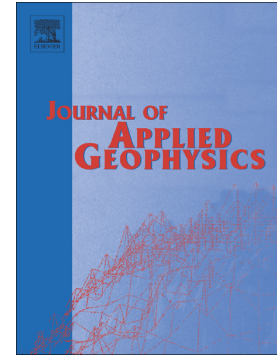
Please cite this article as: C. Jodry, S.P. Lopes, Y. Fargier, et al., 2D-ERT monitoring of soil moisture seasonal behaviour in a river levee: A case study, Journal of Applied Geophysics, https://doi.org/10.1016/j.jappgeo.2019.05.008

2D-ERT monitoring of soil moisture seasonal behaviour in a river levee: A case study

Clara Jodry, Sérgio Palma Lopes, Yannick Fargier, Martin Sanchez and Philippe Côte

Corresponding author: clara.jodry@cnrs-orleans.fr,

Abstract

We present a study of the seasonal behaviour of soil moisture in an old embankment levee by means of 2D DC-electrical resistivity tomography monitoring based on an embedded electrode installation.

We were able to produce seasonal resistivity change models that are compensated for temperature effects using a seasonal temperature profile model. Time-lapse sections of percentage resistivity changes show spatial and temporal overall consistency with seasonal variations of soil temperature. Discrepancies are likely due to the pavement layer that is not well considered in the inversion process as well as to time-lapse inversion pitfalls. Furthermore, a detailed estimation of seasonal moisture content variations could not be given as an accurate calibration of the employed suction probes was not achievable.

Nevertheless, the levee appears to have spatially consistent time variations in soil moisture, clearly influenced by both rainfall and water table and river levels. Future work on developing 3D acquisitions and adding embedded moisture content probes should prove effective to our monitoring design and give a more detailed understanding of the soil moisture seasonal behaviour in the studied stretch of levee.

1. **Introduction**

Piping induced by anomalous seepage is the main cause that may lead to the failure of flood protection structures such as embankment levees (Huang *et al.*, 2014; Cleary *et al.*, 2015). Researchers and levee managers use methodologies to assess and monitor key information on internal condition, such as material and hydraulic properties, including primary studies (e.g. visual inspection), geophysical surveys and geotechnical testing (Fauchard and Mériaux, 2007; Royet *et al.*, 2013; CIRIA, MEDDE, and USACE 2013). However, frequently used geotechnical testing approaches are limited since levees are often heterogeneous and complex structures, particularly in terms of construction material, moisture content and pore pressure distribution, in time, depth and along the length of the levees (Huang *et al.*, 2014; Glendinning *et al.*, 2014). Therefore, geophysical investigations and imaging have been added in many cases to provide high-resolution information of subsurface property changes and stability assessment over long embankment stretch (e.g. Kim *et al.*, 2007; Donohue *et al.*, 2011; Niederleithinger *et al.*, 2012; Perri *et al.*, 2014; Busato *et al.*, 2016; Bièvre *et al.*, 2017; Sentenac *et al.*, 2017).

Among geophysical imaging methods, electrical resistivity tomography (ERT) is a well-established method that is widely applied to embankment levee investigation and seepage detection (e.g. Johansson and Dahlin 1996; Sjödahl *et al.*, 2005, 2010; Weller *et al.*, 2006; Cho and Yeom, 2007; Chinedu and Ogah, 2013; Lin *et al.*, 2014; Loperte *et al.*, 2016). Its sensitivity to soil moisture makes it an appropriate technique for monitoring purposes in the form of time-lapse ERT (TL – ERT) surveys, that allows locating zones with abnormal seepage variations in time (Sjodahl *et al.*, 2008), which is of upmost importance. Indeed, piping originates from areas of low compactness where water seepage increases with time following the detachment and migration of fine soil particles, i.e. internal erosion (Fell and Fry, 2007; Cleary *et al.*, 2015; CIRIA, MEDDE, and USACE 2013).

However, electrical resistivity is highly sensitive to several combined soil properties such as clay content, moisture contents, solute concentration and temperature. Thus, ERT can be used as a proxy to image the spatial and temporal variations of these properties (Telford *et al.*, 1990; Samouëlian *et al.*, 2005). Their combined effects affect the electrical resistivity in different ways and to different extents, which makes interpreting resistivity variations challenging. ERT interpretation is based on empirical relationships between the electrical resistivity and each of these soil characteristics (e.g. Archie, 1942; Keller and Frischknecht, 1966; Gupta and Hanks, 1972; Rhoades *et al.*, 1976; Goyal *et al.*, 1996). In each case, petrophysical relationships are established in order to link geotechnical parameters and temperature measurements to resistivity allowing to quantitatively analyze TL – ERT (Jackson *et al.*, 2002).

In the case of levee monitoring, before identifying zones of anomalous material property variations, one first needs to account for natural seasonal variations in soil temperature and moisture content (Sjodahl *et al.*, 2009). Often, measurements are made using an in-situ probe network (Utili *et al.*, 2015; An *et al.*, 2017; Janik *et al.*, 2017). However, as previously mentioned, these measurements are punctual and probe installation can lead to soil disturbance. Thus, on many occasions, TL – ERT results are qualitatively correlated to water level variations and pluviometry (Panthulu *et al.*, 2001; Lin *et al.*, 2013, 2014; Weller *et al.*, 2014).

In-situ temperature probes allows to build a simple temperature model for the levee that can be used to correct resistivity measurements (Chambers *et al.*, 2014; Glendinning *et al.*, 2015). Moreover, to better understand the resistivity anomalies that can be detected and their implications, TL – ERT measurements can be integrated with geotechnical parameters and

weather measurements (Jackson *et al.*, 2002; Rings *et al.*, 2008; Chamber *et al.*, 2014; Lin *et al.*, 2014; Glendenning *et al.*, 2015).

In our study, we use two-dimensional (2D) TL – ERT based on an embedded electrode installation to monitor the seasonal behaviour of soil moisture in an embankment levee along the Loire in France. TL – ERT based on permanently installed electrodes was introduced by Johansson and Dahlin (1996) on an embankment dam and has been more widely implemented since then (Sjödahl *et al.*, 2008, 2009; Kuras *et al.*, 2009; Ogilvy *et al.*, 2009; Chambers *et al.*, 2014; Weller *et al.*, 2014). The studied site is representative of old fluvial levees as it was first built in the 12th century and has registered many floods and heightening works since then. A special feature of our study is that two parallel lines of electrodes were installed just below the crest, one on the land side and the other one on the river side. The aim was to gain additional insight on the seasonal behaviour of the studied structure. In case the river flooded during the study, the double-line layout was aimed at detecting a water front moving across the levee body. Our study had a twofold objective. The first objective was to assess the feasibility of TL – ERT monitoring based on a permanent electrode system applied to an ancient levee reworked several times over the last centuries and decades. The second objective focused on understanding the seasonal behaviour of soil moisture within the studied levee body. As commonly admitted (e.g. Samouëlian *et al.,* 2005), the electrical resistivity decreases in response to an increase in water content and a drying soil leads to a rise of electrical resistivity. Consequently, we can qualitatively link seasonal resistivity changes to moisture content changes.

The outline of the paper is as follows: first, we present the studied site, the permanent monitoring installation and our methodology, which includes the introduction of a seasonal temperature profile model used to compensate resistivity models. Second, we analyze our monitoring results, including apparent and inverted resistivities as well as direct observation data, and we produce seasonal resistivity changes that are compensated for temperature effects. Then, we show the consistency between the temperature-compensated resistivity changes and the levee soil moisture seasonal behavior. Finally, we discuss results and draw the main conclusions of our study.

2. <u>Studied site</u>

The studied site is a 100 m long embankment levee stretch, which is part of a 50 km long flood defense network along the Loire River in the Authion valley between Angers and Saumur in France. The site has been equipped since 2009 with various permanent sensors meant for experimenting long term monitoring. The geophysical equipment consists in two parallel ERT profiles laid 4 m apart and buried 1.2 m beneath the road structure below the levee crest (Figure 1a). Both profiles comprise 48 aligned electrodes with a 2 m separation. All 96 cable outlets are in direct contact with the embankment soil. Additional instrumentations consist of three piezometers (Pz1 through Pz3, Figure 1) distributed in the transverse direction of the levee within the studied area (Figure 1). Pz3 (9 m deep) and Pz2 (7.6 m deep) are positioned at the edges of the levee crest on the river side and the land side respectively, whereas Pz1 (3.5 m deep) is 3.5 m away from the levee toe on the land side of the levee. Finally, four temperature and suction probes with a recording step of every 4 hours (Watermark® probes, each combining a thermistor and a tensiometer) were placed at depths 1. 2m, 2.5 m, 4 m and 6 m below the crest respectively on the river side of the levee (Figure 1a).

We established a geological section of the site based on previous geotechnical drilling campaigns and the overall geological setting of the area (Figure 1b). The levee body, formed

of compacted silty-clayey sand, is 4.5 m high from the land side levee toe and 6 m high from the riverbank side. Alluvial Loire River deposit form the natural levee foundation, comprising (from top to bottom) an approximate 2 m thick permeable layer of clayey-sandy silt, a 6 m thick impervious clay formation and a confined aquifer sand formation. Finally, the bedrock is made of Turonian chalk. From previous 2D ERT inversion results and direct resistivity measurements on core samples, an average resistivity value of about 60 Ω.m for the earth fill layer and of 20 Ω.m for the alluvial layer (for both the clayey-sandy silt and the clay formations) was estimated.
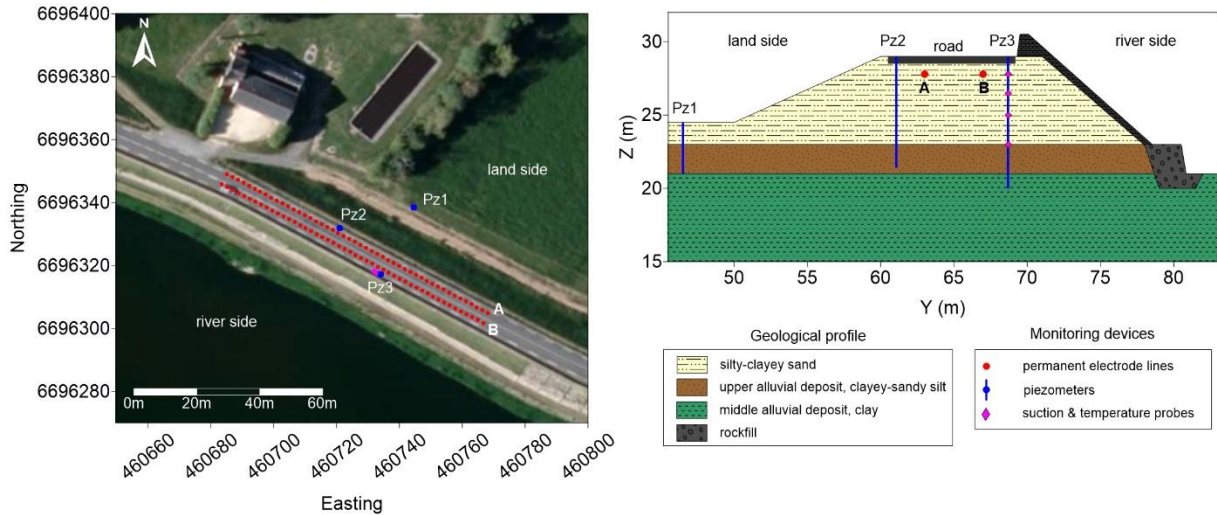

Figure 1: a) Satellite view of the site (in Lambert 93 coordinates, ©Google Earth) and b) Geological cross-section of the Loire river levee and natural foundation with the permanently installed ERT lines and additional monitoring devices. The thick dark grey parts represent the road structure and the masonry revetment on the crest and the river side slope respectively.

Regarding the environmental conditions of this study, it is worth mentioning the following information. First, in a previous study of the same site, Jodry *et al.* (2017) reported the presence of shallow and regularly spaced anomalies (approx. every 30 m) below the levee toe on the river side, possibly due to local features in consistency with past reinforcement works. They showed that these anomalies had significant 3D effects on the 2D ERT images yielded by both ERT lines, and most particularly for the one on the river side. Second, the river did not flood during the period of the study, and merely showed average seasonal level variations.

3. **Methodology**

3.1. Data acquisitions

The permanent ERT setup was used to collect one acquisition per month based on a Wenner-Schlumberger protocol (Dahlin *et al.*, 2004) comprising 997 measured apparent resistivities on each of the electrode lines using a SYSCAL Pro® (IRIS Instruments) resistivity meter. Data quality was deemed very good according to i) low and stable contact resistances, ii) low stacking discrepancy and iii) smooth lateral apparent resistivity variations for a given electrode spacing (no spikes).

Concurrently with each monthly ERT acquisition, additional recordings were manually taken as follows: i) water level and electrical conductivity were acquired in the piezometers and the Loire river; and ii) soil surface temperature was measured with a portable probe (estimated measurement depth is 0.1 m). Finally, daily rainfall data were collected from a weather station (Météo-France national meteorological service) located 18 km away from the studied site.

3.2. ERT processing

Accurate geometric factors were generated through a 3D numerical model of the levee (using the COMSOL Multiphysics® finite element environment) to avoid misinterpretation from 3D effect artifacts (Rücker *et al.* 2006; Lin *et al.*, 2014). In the levee model, the embankment topography, the actual positions of both lines of embedded electrodes and the actual height of the Loire river at the time of each ERT acquisition are considered (Marescot *et al.,* 2006; Wiwattanachang and Giao, 2011; Jodry *et al.,* 2017).

The observed apparent resistivity datasets were inverted using RES2Dinv commercial software (version 3.59) (Loke and Barker, 1996). The inversion scheme is based on a least squares smoothness constrained iterative optimization algorithm (Constable *et al.,* 1987; De Groot-Hedlin and Constable, 1990). Here, we used the L2 norm (i.e. Menke, 1984; Loke, Acworth and Dahlin, 2003) to generate a smooth resistivity model. This was done in conformity with a priori knowledge from previous borehole data that indicate a progressive vertical resistivity variation and comparatively smaller horizontal variation between boreholes.

Several techniques proposed for the time-lapse inversion of time series of data (e.g. Hayley *et al.* 2011; Karaoulis *et al.* 2014) use more or less sophisticated algorithms that make use of temporal and spatial constraints to reliably reconstruct subsoil resistivity changes with as limited artifacts as possible. Here we used a smoothness constraint applied on temporal variation through a simultaneous "cascade time lapse inversion" (e.g. Miller *et al.*, 2008; Hayley *et al.* 2011) that is more adapted to seasonal resistivity variations (Sjodahl *et al.*, 2008).

We assessed the convergence level of the inversion based on the relative root mean square error as defined in Gupta *et al.* (1997) and simply denoted 'RMS' in this paper.

3.3. Causes for seasonal resistivity variations

Resistivity variations are driven by the combined effects of several soil properties. Since this fluvial levee is not exposed to permanent hydraulic head and no flooding conditions occurred over the span of the study period of time (2009-2016), it was assumed that clay content changes (due to internal erosion phenomena) were negligible or even null. Moreover, the clay content in the fill material of the levee body is not sufficient for porosity changes due to shrink-swell phenomenon to occur. Therefore, in this study, we assume that only soil temperature and moisture content show seasonal variations within the levee body and foundation.

3.4. Temperature profile modelling and compensation

As previously mentioned, our aim is to show how resistivity changes in the levee body relate to soil moisture changes. In this context, it is important to retrieve resistivity changes that are free from temperature effects, as emphasized by Hayley *et al.* (2007). To compensate the temperature contribution to resistivity changes we assume the linear empirical model state introduced by Keller and Frischknecht (1966) for a variety of subsurface materials, with a standard temperature of 18 °C:

$$\rho_T = \frac{\rho_{18°C}}{1 + m(T - 18)} \qquad (2)$$

where ρ_T is the bulk electrical resistivity of a medium at temperature T [°C]. $\rho_{18°C}$ is the resistivity at the standard temperature (18°C) and m is fractional change in bulk electrical resistivity per degree Celsius, which is assumed here to be approximately 0.025°C^{-1} (i.e. assuming a variation of 2.5% in resistivity per degree Celsius, regardless of soil type) (Keller and Frischknecht, 1966).

Hayley *et al.* (2007, 2010) demonstrated that temperature effects on bulk resistivity can be approximately corrected for and compared two temperature compensation approaches for

TL – ERT imaging: the straightforward approach based on compensating resistivities after inversion of raw data and a competing approach based on inverting temperature-compensated data. The latter implies a more complex process that includes forward simulations. Here we apply the former approach as used by Brunet, Clément and Bouvier, 2010; Pellicer et al, 2012; Chambers et al., 2014; Glendenning et al., 2014) in the same context.

The following sinusoidal expression was proposed to represent seasonal variations of vertical temperature profiles in the subsurface (Kappelmeyer, 1957; Musy and Soutter, 1991). Such variations are governed by general heat transfer laws and therefore behave as a damped thermic wave in the ground:

$$T(z,t) = \bar{T}_0 + A_0 e^{-\frac{z}{d}} \sin\left(\omega t - \omega t_0 - \frac{z}{d}\right) \tag{3}$$

where $T(z,t)$ denotes the average temperature at date t [days] and depth z [m] below the levee crest (note that the z is positive downwards with z = Z – 29, Z [m] being is the elevation as previously used and Z = 29 m at the levee crest), $\bar{T}_0$ [°C] is the yearly mean temperature of air (at the ground surface), A_0 [°C] is the yearly amplitude of the air temperature variation, which was set to 7.5°C according to the closest meteorological station (© Méteo France data). The attenuation of the wave amplitude increases with depth at the rate $e^{-\frac{z}{d}}$, where d is the characteristic penetration depth of the thermic wave. The delay of the temperature variations increases with depth as well, as imposed by the phase lag $\omega t_0 + \frac{z}{d}$ in the sine term, where $\omega = \frac{2\pi}{365}$ is the angular frequency for a one-year period (365 days), t_0 is the origin of the sine function which happens here to be very close to April 23rd, 2014, for all depths. The characteristic penetration depth depends on the thermal properties of the subsoil and on the frequency ω (Musy and Soutter, 1991). For a yearly frequency, d should range from 1.41 m (dessicated clay) to 2.75 m (water saturated sand).

Equation (3) is the sinusoidal approximation of the complex thermal regime occurring in a subsoil and stands under some assumptions. In particular, heat transfers are supposed to be unidirectional, the yearly average temperature is assumed to be constant with depth (equal to that of air) and the spatial and temporal variations of soil thermal properties are considered negligible. The latter assumption is certainly the most difficult to ensure. In the case of our study, it was not possible to fit a single model to all our temperature data jointly, probably due to local conditions and high vertical variability in terms of material type (from top to bottom: road structure, loamy sand embankment, clayey-loamy alluvions) and water saturation levels (which also vary over the seasons).

Alternatively, we adapt equation (3) to the following form of vertical-temporal temperature profiles:

$$T(z,t) = \bar{T}(z) + A_0 e^{-\frac{z}{\alpha(z)d}} \sin\left(\omega t - \phi - \frac{z}{\beta(z)d}\right) \tag{4}$$

where $\alpha(z)$ and $\beta(z)$ are dimensionless coefficients that allow accounting for soil differences in attenuation and delay, and $\bar{T}(z)$ is the yearly average temperature at depth z.
It should be noted that although Musy and Soutter (1991) and Chambers *et al.* (2014) use coefficient values $\alpha = \beta = 1$, Brunet *et al.* (2010) and Pellicer *et al.* (2012) rather use $\alpha = 1$ and $\beta = 4$ at all depths, thus leading the way to some model adaptability.

After fixing the characteristic penetration depth to the expected average value $d = 2m$, coefficients $\alpha(z)$ and $\beta(z)$ were determined by fitting the model in equation (4) to the temperature data at each depth separately. Although time unit is in days here, we used monthly mean temperature for fitting this temperature model. Adjusted values of $\alpha(z)$ and $\beta(z)$ coefficients at the depths of the temperature probes are given in Table. 1.

Table 1. Adjusted values for surface and probes' depth of the yearly mean temperature $\overline{T}_0(z)$ and the attenuation parameters α and β for the amplitude and phase lag respectively.

Elevation (m)	Depth (m)	$\overline{T}$ (°C)	α	β
28.9	0.1	13.0	0.8	1
27.8	1.2	16.4	12	5
26.5	2.5	16.0	5.6	3.6
25	4.0	15.3	4.6	3.2
23	6.0	14.6	3.9	2.8

This adjustment was carried out under customized Matlab routines to ensure a minimal misfit between modeled and measured data (Figure 2.a, plain and dotted lines respectively). A reasonable fit quality was achieved at the five depths corresponding to the soil surface temperature recording (at depth 0.1 m) and the four installed temperature probes (at depths 1.2m, 2.5m, 4.0m and 6.0m). Although the four permanently installed temperature probes used in this study (section "studied site") have a limited resolution (1°C), the usual sinus-like soil temperature trends can be seen, with a decrease in amplitude variations and an increase in phase delay with depth.

Finally, since model parameters $\overline{T}$, α and β depend on depth z, we applied linear interpolation in between the fitted values in order to retrieve estimated parameters at the required resistivity inversion depths and be able to compensate all inverted resistivities for temperature effects. The final temperature models, for each month and resistivity inversion depths are displayed Figure 2.b.
Although the embedded temperature probes are closer to the river side of the levee (Figure 1), we used the same temperature profile model for compensating both inverted resistivity sections (river side and land side electrode lines).
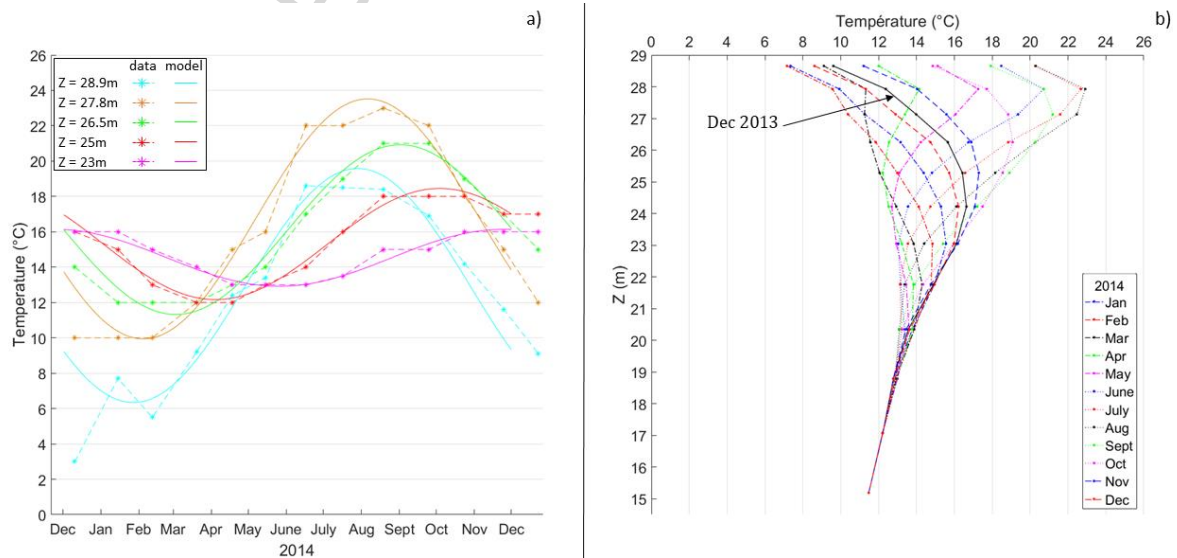
Figure 2. a) Observed and modelled soil temperatures for surface and subsurface probes at five depths; b) Modelled soil temperature at each resistivity inversion depth for the reference date, December 2013, and each month of year 2014.

4. <u>Analysis of results and temperature compensation</u>

In fulfilling our objective to understand the seasonal behaviour of the levee soil over the span of a year, and more specifically to relate TL – ERT results to soil moisture changes, we first briefly analyze the seasonal changes in measured apparent resistivities. Then we present changes in inverted resistivities in the light of direct observation data and we compensate these changes for measured changes in temperature. Finally, we link temperature-compensated resistivity changes to seasonal trends of soil moisture changes.

4.1. Basic analysis of apparent resistivity data

Here we focus on the apparent resistivities and their seasonal evolution. Figure 3 presents the apparent resistivity values from the land side electrode line for various quadrupole configurations and spacings. Data from the river side electrode line are not shown here as they follow similar trends.

The left column of Figure 3 shows the calculated mean of year-round apparent resistivity for all month ± the standard deviation for each position X for 2014. The smallest electrode spacing (AB = 6 m with a = 2 m and n = 1) shows that the yearly magnitude of apparent resistivity variations is about 20 Ω.m. This amplitude progressively decreases while AB increases until a minimum variation of 5 Ω.m for AB = 44 m (a = 4 m, n = 5). We note that temporal variations in apparent resistivity show some spatial consistency along the levee as they do not strongly depend on the lateral position (X) along the profile.
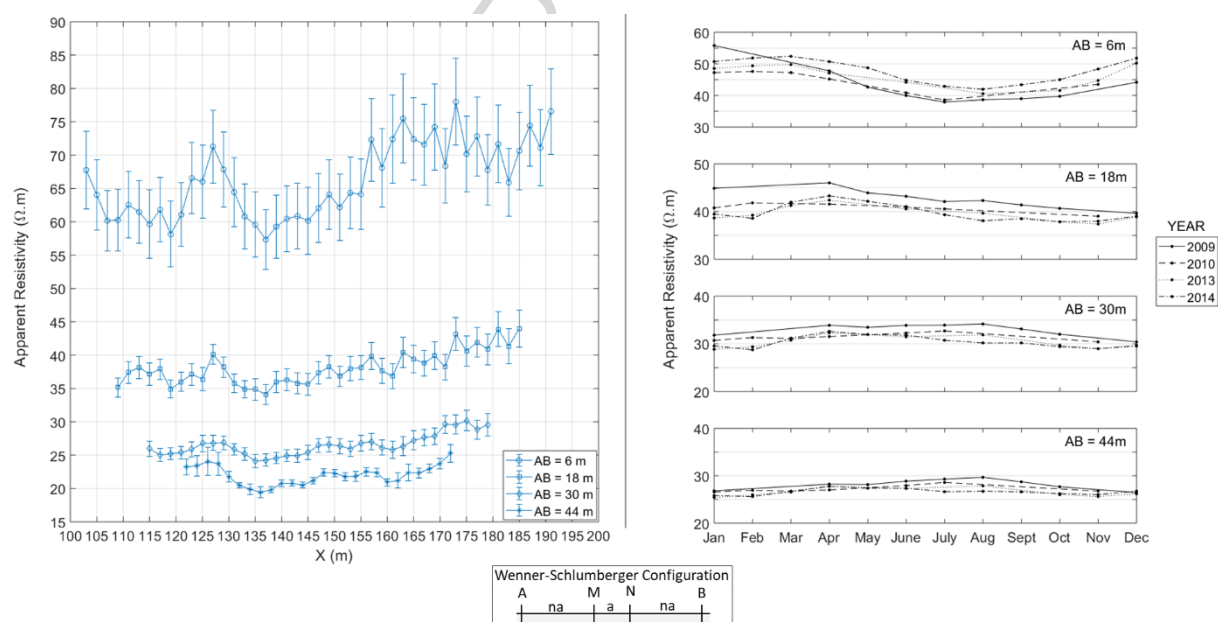

Figure 3: Raw Wenner-Schlumberger apparent resistivity (Ω.m) data acquired with the electrode line situated on the land side. Left: Selected apparent resistivity profiles for each monthly acquisition in 2014; Right: Mean apparent resistivity for each selected profile and monthly acquisition for years 2009, 2010, 2013 and 2014.

In order to assess the trends of these variations over the span of years, we calculated the mean apparent resistivity for each AB electrode spacing and each monthly acquisition. These mean values plotted against months in a year allow us to observe their evolution during the four seasons for different years, 2009, 2010, 2013 and 2014 on the right column of Figure 3. We show that for the smallest lengths of quadrupoles with AB = 6 m (a = 2 m, n = 1), the average apparent resistivities are higher in autumn and winter and lower in spring and summer. In the case of intermediate AB lengths of 18 m (a = 2 m, n = 4), seasonal variations in mean apparent resistivity are generally lower. Finally, for larger electrode spacings with AB = 30 to 44 m (a = 6 m, n = 2, a = 4 m, n = 4 and 5, then a = 6 m, n = 4) mean apparent resistivities show relatively little variations over the seasons for each considered year.

Overall, the maximum seasonal variations are yield for the smallest spacing, with maximum and minimum apparent resistivities in the winter and summer respectively. Hence, the levee subsoil seems to partially respond to seasonal weather conditions and with similar amplitudes each passing year.

4.2. Time-lapse ERT results without temperature compensation

A more in-depth analysis is presented here based on the 2D inverted resistivity tomographies for the land and the river sides of the levee (Figure 4, left and right columns respectively).

These images show the area of interest, from elevation Z = 29 m (levee crest) down to elevation Z = 15 m, which covers the levee body (embankment) and the first two alluvial layers (the permeable clayey-sandy silt layer and the impervious clay formation) (Figure 1). The confined sand aquifer formation just below should not exhibit significant temporal changes considering that it stands significantly below the water table level and river level all year round and is therefore assumed to be permanently saturated. Moreover, the temperature changes in this formation are considered negligible for it is situated at a depth of about 9 m below the levee toe and 14 m below the levee crest. Furthermore, we do not expect to have sufficient resolution at such depths where inversion results might lead to misinterpretation.

The top two tomographies are the inverted resistivities obtained for December 2013, which is the reference date (ρ_{ref}). Both models represent results from the 5th iteration and an RMS error of 1.35 % and 2.2 % for the land and river side respectively. The top layer with an average resistivity of 60 Ω.m reflects the 5-6 m thick embankment, which appears homogeneous along the crest, for both levee sections. The resistivity level decreases rapidly between elevations 26 m and 24 m to attain approximately 20 Ω.m and 15 Ω.m int the silt and clay alluvial deposits respectively. On the river side, the resistivity transition is not even, which is most possibly related to 3D effects due to local features beneath the levee toe on this side, as mentioned in section "Studied site" (see also Jodry *et al.*, 2017). Based on borehole data, it was clearly demonstrated that the ERT image on the river side contained inversion artifacts, and that the actual interface between the embankment and the alluvial layers was most likely to be horizontal, as on the land side.

The other ERT images presented in Figure 4 show time-series sections of percentage change in model resistivity for each month in year 2014 (ρ_t). The RMS values, at the 5th iteration, are comprised between 1.38 % and 3.8 % for all tomographies. For each inversion cell, the percentage change (%) in inverted resistivity is calculated as:

$$\frac{\Delta\rho}{\rho} = \frac{(\rho_t - \rho_{ref})}{\rho_{ref}} \times 100 \tag{5}$$

The time-lapse inverted models obtained for the land and river side ERT lines (Figure 4, left and right columns respectively) exhibit quite similar seasonal resistivity changes. Thus, it should be noted that the inversion artifacts previously mentioned (on the river side reference

resistivity image) only induce limited contamination in the time-lapse percent images. This is an important finding for the feasibility of TL – ERT monitoring applied to this levee stretch.

Seasonal resistivity variations are in the range of –30 % to +30 % from the reference resistivity section in December 2013. In the upper layer ($Z > 25$ m), the levee is slightly more resistive in January and February 2014, compared to December 2013. Then we observe an evolution towards decreasing resistivities from March 2014 until August 2014 that spreads from the top down to the bottom over time. From August to December 2014, percentage resistivity changes in the upper levee layer show a progressively increasing trend and exhibit some spatial variability towards the end of the year.

The resistivity changes at the base of the embankment body and in the clayey-sandy silt deposit layer (between $Z < 25$ m and $Z > 21$ m) generally show an opposite behaviour, with percentage resistivity changes ranging from –20 % (February) to +25 % (May and June) and back to lower values towards the end of the year. The clay formation, below $Z = 21$ m, follows the same pattern as the silt layer with lower percentages resistivity changes, comprised between –10 % an +10 %.

From these inverted results, we conclude that this stretch of ancient levee in the Authion valley seems to follow 'cyclic' resistivity variations over the course of year 2014 with reverse behaviours for upper ($Z > 25$ m) and lower ($Z < 25$ m) layers of the embankment and its foundations. Thanks to the similar results on both time-lapse series (land and river sides), we also conclude that this levee stretch shows a homogeneous seasonal behaviour in the transverse direction. Finally, although it is likely that the levee body and the natural foundation do not fully recover their original state after a full year, we notice that December 2014 results in Figure 4 exhibit some high percentage values and large lateral variability. We suspect part of this variability to be due to numerical instability in long-term TL – ERT inversion.
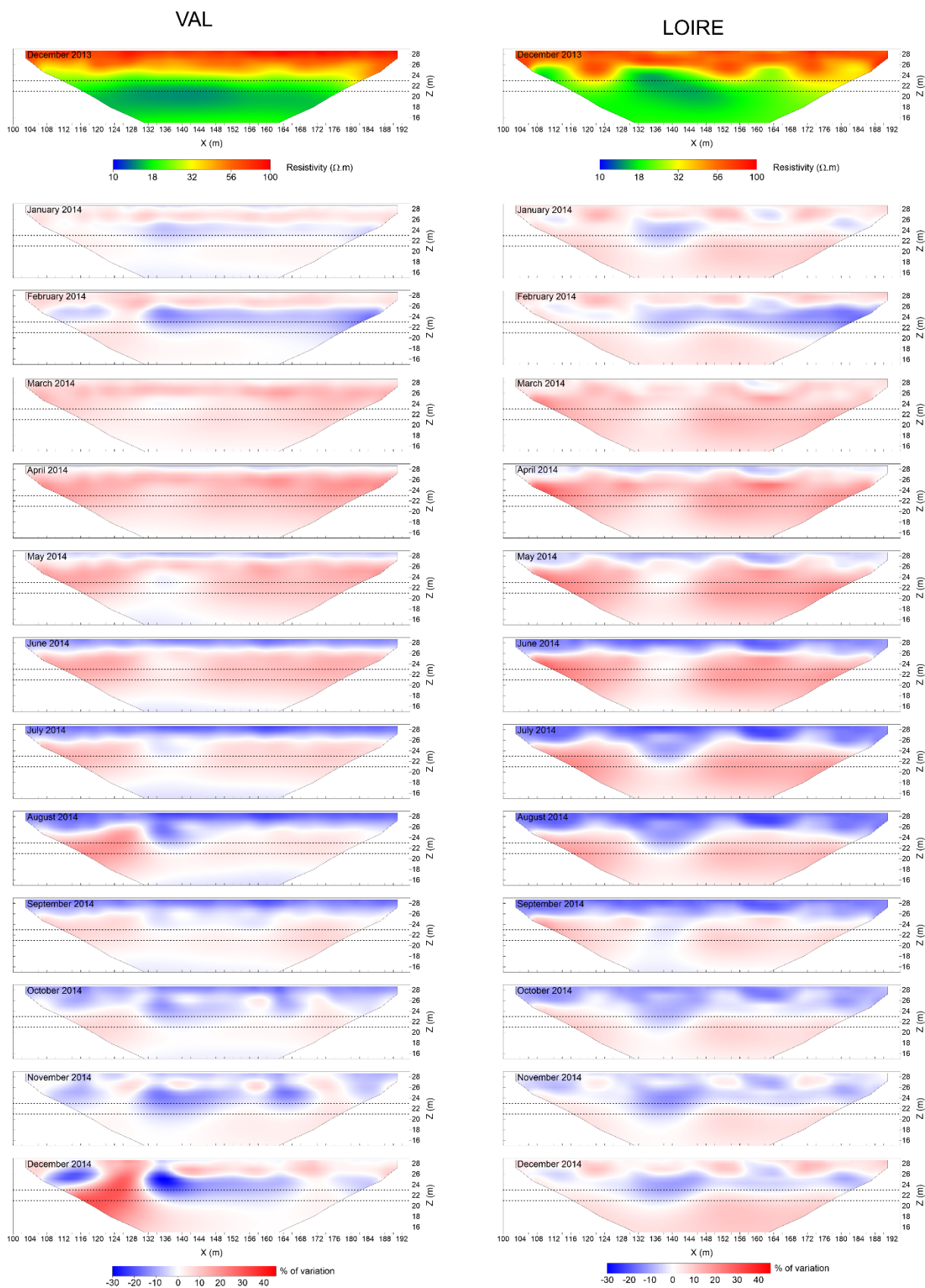
Figure 4. 2D inverted resistivity tomographies for the reference date of December 2013 (top sections) and percentage resistivity change sections from "cascade" inversions for a) the land side and b) the river side. The dotted lines represent the top of each alluvial layers estimated according the geotechnical data (Figure 1).
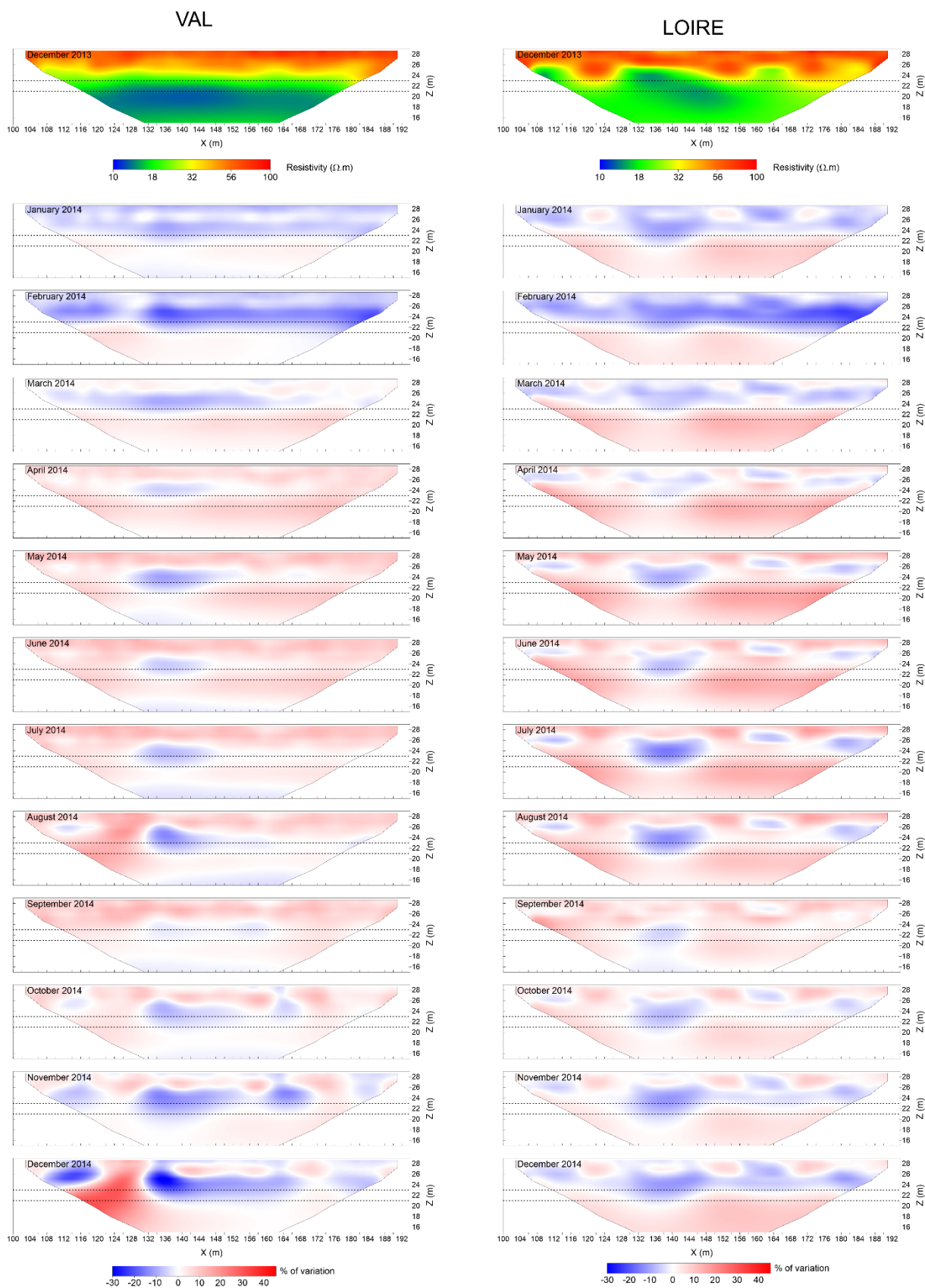
Figure 5. 2D inverted resistivity tomography corrected of the modelled temperature (Figure 2.b) for the reference date of December 2013 (top sections) and percentage resistivity change sections from "cascade" inversions for a) the land side, and b) the river side. The dotted lines represent the top of each alluvial layers estimated according the geotechnical data (Figure 1).

4.3. Time-lapse ERT results compensated for temperature variations

Figure 5 presents the reference 2D inverted resistivity models (Dec. 2013) and the subsequent monthly sections of percentage change in model resistivity compensated for the effect of temperature based on the modelled temperature (Figure 2.b) and application of Equation 2.

The inverted resistivity tomographies, obtained for December 2013 with and without temperature compensation (top row of Figure 4 and Figure 5 respectively), do not show significant differences. Yet, percentage resistivity change sections are quite modified. This is especially noticeable for the upper levee body layers (Z > 25 m) which are more impacted by temperature variations.

Indeed, for the upper layers (Z > 25 m), percentage changes in resistivity are generally of opposite sign compared to that of non-compensated results (Figure 4). This contrast between non-compensated and compensated resistivities progressively decreases downwards (from Z = 25 m to Z = 15 m) as the temperature compensation magnitude decreases. We also note that, for all elevations, the contrast tends to vanish towards the end of year 2014. This is likely due to the fact that temperature profiles, and thus temperature compensations, tend to are very similar for December 2013 and December 2014 (Figure 2.b).

Once again, the sections of percentage resistivity change for the land and river sides of the levee (Figure 5, left and right columns respectively) show similar comportments and amplitudes throughout the year, despite some local discrepancies. Although one could have expected this similarity, based on the similarity previously stated for the non-compensated ERT results (Figure 4), it is important to note that the seasonal changes within this stretch of levee exhibits spatial consistency to some extent. This statement is made possible thanks to the double ERT line installation.

Overall, we distinguish again a cyclic behaviour of the resistivity changes with variable comportment with depth. The beginning of year 2014 induces a decrease in resistivity (January and February) then the levee body becomes more resistive compared to December 2013 and remains more resistive throughout spring and summer (from March to August). Autumn and the beginning of winter (September to December) prompt a new decrease in resistivity.

In sum, temperature-compensated resistivities show significant seasonal variations throughout the year, although the yearly amplitude is smaller than for non-compensated resistivities. One can reasonably associate these compensated resistivity changes to soil moisture variations. However, one also notes that the resistivity changes show some lateral variability for each depth, depending on the side of the levee (land side or river side) and the period of the year. Possible interpretations for this are discussed later.

In order to highlight the overall seasonal behaviour, we calculate the average percentage resistivity changes at seven selected elevations in the levee body, both with and without temperature correction, and plot them against time (Figure 6). The selected elevations are the depths of the discretization cell layers as designed by the inversion software we used, i.e. Z = 27.9, 26.2, 25.3, 23.0, 20.3, 17.0, 15.2 m.

For Figure 6.a and c, the soil shows resistivity variations in the range of –20 % to 15 %. Yet again, the duality between seasonal behaviour in the near surface and in the deeper layers is clearly visible (as for Figure 4). Figure 6.b and d display less resistivity variations with a range of 15 % in all. We note an abrupt decrease in resistivity in February that seems independent from temperature variations since it can be seen on all four profiles (Figure 6). We suspect it to be the result of an abrupt change of another soil parameter. Furthermore, we can observe that

the deeper layers, at Z =17 m and Z = 15.2 m, show resistivity variations close to 0 % with and without temperature correction (Figure 6).
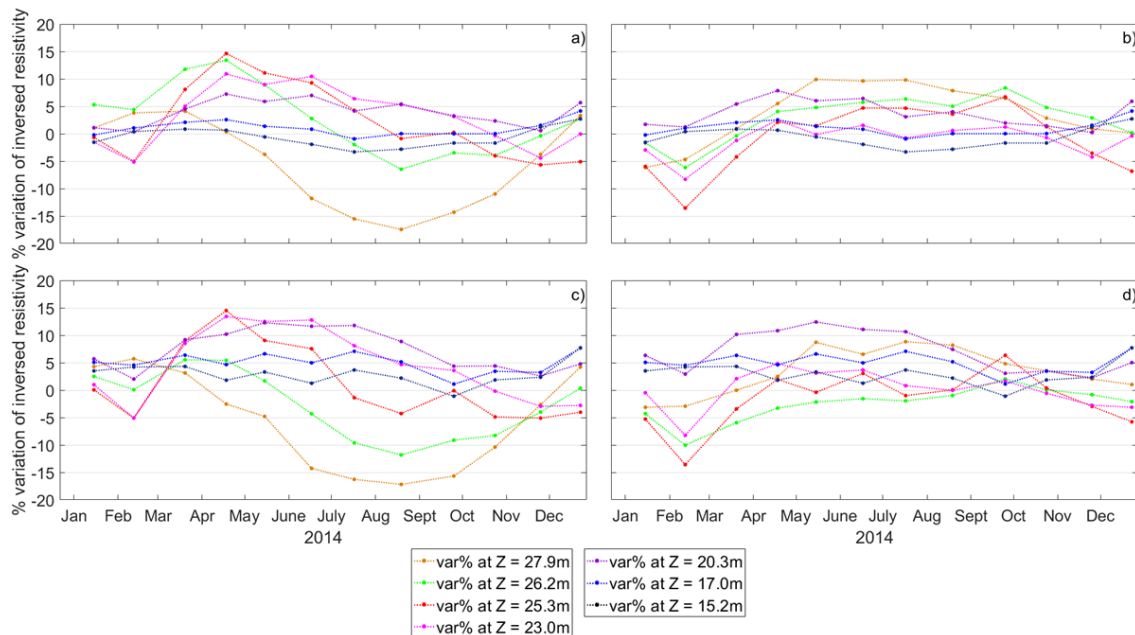

Figure 6. Time-series graphs showing average percentage resistivity changes with time at seven different elevations in the levee body, for the land (a. and b.) and the river (c. and d.) sides of the levee, and for non-compensated (a. and c.) and temperature-compensated (b. and d.) resistivities.

As expected from the previous results, average resistivities from the river and the land side ERT lines show very similar seasonal trends for each depth, both for compensated and non-compensated resistivities.

4.4. Consistency between resistivity changes and soil moisture seasonal behaviour

In this section, we associate the remaining resistivity changes to changes in the subsoil moisture level. We compare our resistivity results to the direct observation data (see Section "Methodology, data acquisition") that are linked to moisture content changes in the subsoil.

Figure 7.a displays the suction measurements at four depths in the levee (Figure 1). To correlate suction to moisture content, a laboratory calibration would be necessary. However, such calibration is difficult to achieve and is highly soil-dependent. Indeed, the water retention curve of a natural porous material always has marked hysteresis phenomena during periods of dewatering or moistening of the material. Our calibration attempts did not yield relevant results. Therefore, seasonal variations in suction can qualitatively translate as the higher the suction is, the drier is the soil. Conversely, weak values of suction indicate that the soil is saturated or close to saturation.

Data from the shallowest probe (Z = 27.8 m and Z = 26.5 m) mostly show variations that are tied to pluviometry (Figure 7.b) with a short temporal shift due to infiltration time in the soil and water migration towards the water table. It should be emphasized that the meteorological data presented here was issued from a meteorological station situated 18 km north of the studied site. Nonetheless, we observe that rainy events induce a drop of suction in the upper layer of the levee body (Figure 7.a).

Data from the deepest probes (Z = 26.5, 25 and 23 m) responses are more closely linked to the water table level. This statement is illustrated in the period of February to March 2014: The water level rose up to elevation Z = 24.3 m (above the deepest probe level, Figure 7.c) and one can see a simultaneous and significant decreases of suctions (Figure 7.a). In that, the suction response to water level is more rapid than for rain infiltration variations. We also observe that between April and October the water table level and suction remain nearly constant. It is only in December with the rise of the water table that we see another suction decrease at the deepest levels.
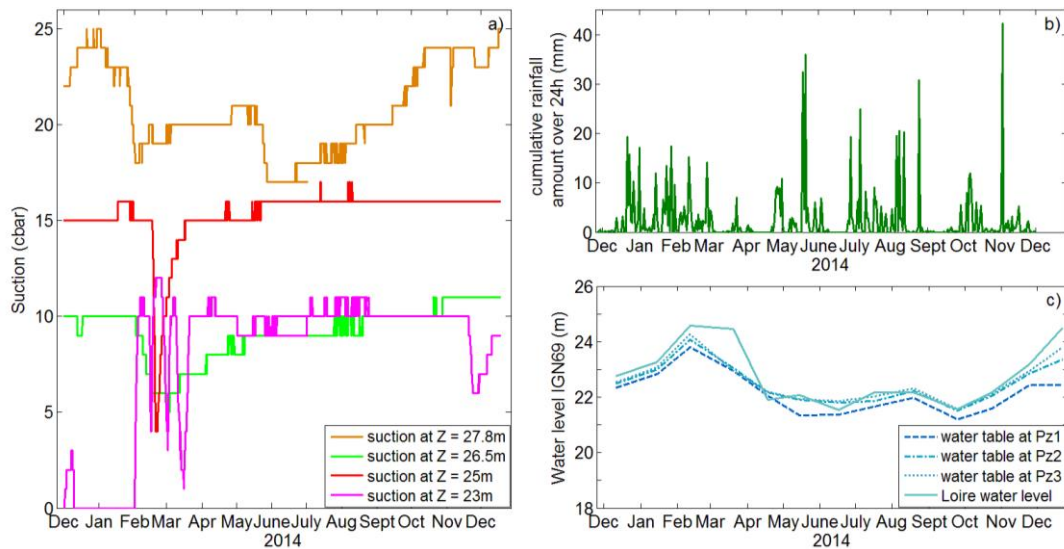

Figure 7. Time-series graphs of direct observations over the year 2014 for: a) Suction at four depths within the levee body; b) Daily cumulative rainfall recording (MeteoFrance ©) and c) Monthly water table levels at piezometers Pz1 through Pz3 (Figure 1) and monthly measured level of the Loire river.

We have shown that suction variations (Figure 7.a) are indeed directly linked to moisture seasonal changes. We now correlate those measurements to the percentage change of mean resistivity on the river side seen in Figure 6.d (Figure 8).
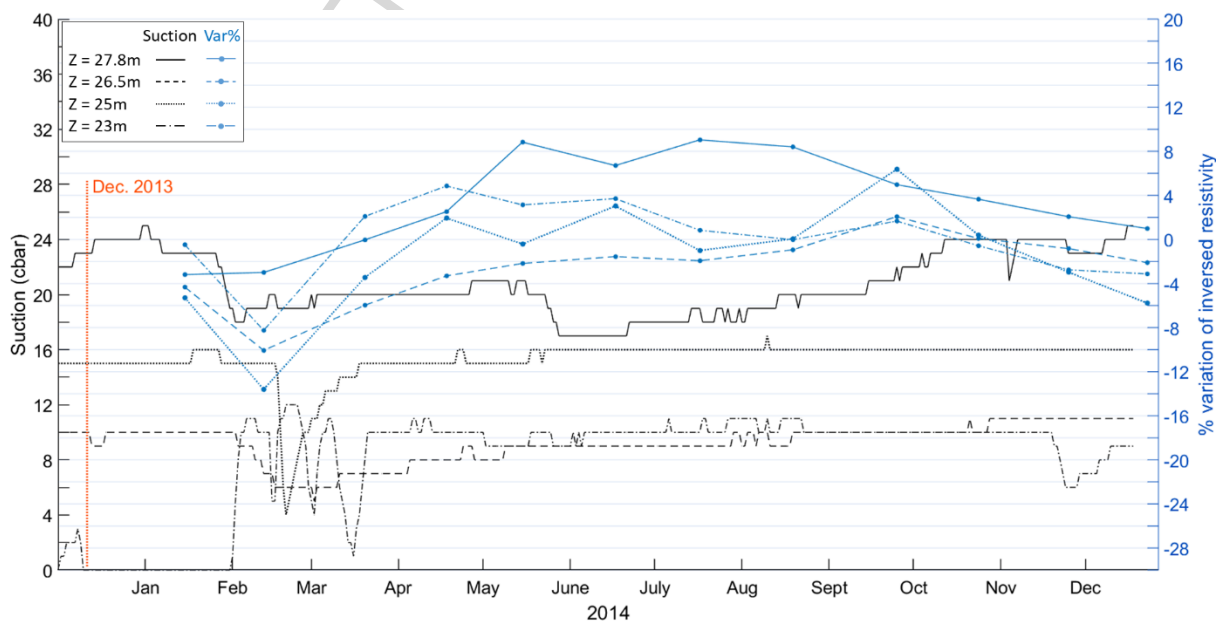
Figure 8. Comparison of time-series graphs of suction direct measurements within the levee body and time-series graphs showing average percentage resistivity changes for temperature-compensated resistivities of the river side of the levee, over the year 2014 and at four depths.

Figure 8 shows a clear correlation between resistivity variation and moisture content for the soil situated below $Z = 26.5$ m. Indeed, the augmentation of moisture content, due to the water table rise, induces both a suction and a resistivity drop (of –8 to –15 %) at the beginning of year 2014. As the moisture content stabilizes over the year 2014, so do the resistivity variations which are in the range of ±6%.

In contrast, the shallowest layer right below the levee crest, at about $Z = 27.8$ m, shows a conflicted behaviour between the moisture content and the resistivity variations. Indeed, moisture content tends to increase (as suction decreases) with resistivity (from –3% to +9%) when it should, theoretically, be the opposite. This contradictory behaviour will be discuss further in the next section.

4.5. Discussion on remaining local variability in the time-lapse resistivity sections

Time-lapse sections of percentage resistivity changes show spatial and temporal variations linked to variations of soil temperature and moisture. However, these same sections exhibit some local variabilities that cannot not linked these seasonal variations.

We believe that they are, in part, due to time-lapse inversion pitfalls and the effects of construction features at the toe of the levee (Jodry *et al.*, 2017). Indeed, small input data variations may lead to significant image variations because of equivalence issues, particularly for datasets spanning over long periods of time and showing low changes. Only more advanced time-lapse inversion schemes, e.g. with a priori information constraints may mitigate such instability (Clément *et al.*, 2009; Carey *et al.*, 2017).

Other bias can have also been induced by our temperature model based on temperature data at only five different depths and used it to compensate the inverted resistivities at all depths. Although this allowed a plausible model for the time varying vertical temperature profile, it is still to be proved that such a temperature profile is the same along and across the levee, especially considering the 3D shape of this levee and the location of the probes that are closer to the southern side of the levee.

Finally, we also believed that the pavement layer is not well considered as it induces a different behaviour in the shallow layers ($Z > 27$ m) as seen in Figure 5 and Figure 8.

5. **Conclusion**

In our study, we used 2D TL – ERT based on a permanent electrode installation to monitor the seasonal behaviour of soil moisture in an earthen levee along the Loire River in France. The studied site illustrates typical ancient fluvial levees, which are more heterogeneous and complex than recent embankment dikes. The permanent monitoring installation is based on two parallel lines of electrodes below the crest and additional series of piezometers and embedded probes for direct soil and water property measurements. A model of vertical-temporal soil temperature profile was empirically adjusted based on direct measurements. It was applied to compensate our time-lapse ERT results for temperature effects, under the assumption that this model does not vary significantly along and across the levee body.

The monitoring feasibility was demonstrated based on high quality long-term ERT data thanks to the permanent electrodes in direct contact with the levee soil. Moreover, time-lapse sections of percentage resistivity changes show spatial and temporal overall consistency with seasonal variations of soil temperature and moisture. Local variability in these sections cannot be fully

explained without additional field evidence, and it was suggested that part of it is due to time-lapse inversion pitfalls.

These time-lapse results covering the double 94 m long ERT line installation allowed a better understanding of the soil moisture seasonal behaviour in the studied stretch of levee. Within an average hydro meteorological year (no flood), the levee appears to have somewhat spatially consistent time variations in soil moisture, clearly influenced by both rainfall and water table and river levels. Detailed estimation of seasonal moisture content variations could not be given at this stage as an accurate calibration of our suction probes was not achievable.

Prospects include adding embedded water content probes to our monitoring design and testing it over long periods of time that possibly host higher hydraulic load or flood events. Coupled with additional calibrations on soil samples, it could enable us to provide quantitative evaluation of seasonal variations of the moisture content from resistivity variation. Furthermore, even though 2D inversion is common practice for levee survey, research directions would consist in developing 3D acquisitions and joint inversion of both in-line and cross-line datasets as well as dedicated time-lapse inversion constraints.

Acknowledgments

References

An, N., Hemmati, S., Cui, Y., 2017. Numerical analysis of soil volumetric water content and temperature variations in an embankment due to soil-atmosphere interaction. Comput. Geotech. 83, 40–51. https://doi.org/10.1016/j.compgeo.2016.10.010

Archie, G.E., 1942. The electrical resistivity log as an aid in determining some reservoir characteristics. Trans. AIME 146, 54–62. https://doi.org/10.2118/942054-G

Bièvre, G., Lacroix, P., Oxarango, L., Goutaland, D., Monnot, G., Fargier, Y., 2017. Integration of geotechnical and geophysical techniques for the characterization of a small earth-filled canal dyke and the localization of water leakage. J. Appl. Geophys. 139, 1–15. https://doi.org/10.1016/j.jappgeo.2017.02.002

Brunet, P., Clément, R., Bouvier, C., 2010. Monitoring soil water content and deficit using Electrical Resistivity Tomography (ERT) - A case study in the Cevennes area, France. J. Hydrol. 380, 146–153. https://doi.org/10.1016/j.jhydrol.2009.10.032

Busato, L., Boaga, J., Peruzzo, L., Himi, M., Cola, S., Bersan, S., Cassiani, G., 2016. Combined geophysical surveys for the characterization of a reconstructed river embankment. Eng. Geol. 211, 74–84. https://doi.org/10.1016/j.enggeo.2016.06.023

Carey, A.M., Paige, G.B., Carr, B.J., Dogan, M., 2017. Forward modeling to investigate inversion artifacts resulting from time-lapse electrical resistivity tomography during

rainfall simulations. J. Appl. Geophys. 145, 39–49. https://doi.org/10.1016/j.jappgeo.2017.08.002

Chambers, J.E., Gunn, D.A., Wilkinson, P.B., Meldrum, P.I., Haslam, E., Holyoake, S., Kirkham, M., Kuras, O., Merritt, A., Wragg, J., 2014. 4D electrical resistivity tomography monitoring of soil moisture dynamics in an operational railway embankment. Near Surf. Geophys. 12, 61–72. https://doi.org/10.3997/1873-0604.2013002

Chinedu, A.D., Ogah, A.J., 2013. Electrical Resistivity Imaging of Suspected Seepage Channels in an Earthen Dam in Zaria, North-Western Nigeria. Open J. Appl. Sci. 03, 145–154. https://doi.org/10.4236/ojapps.2013.31020

Cho, I.-K., Yeom, J.-Y., 2007. Crossline resistivity tomography for the delineation of anomalous seepage pathways in an embankment dam. Geophysics 72, G31–G38. https://doi.org/10.1190/1.2435200

CIRIA, MEDDE (Ministère de l'Écologie du Développement durable et de l'Energie), USACE (US Army Corps of Engineers), 2013. The International Levee Handbook. CIRIA, p 4; p 124-125; p 156-175.

Cleary, P.W., Prakash, M., Mead, S., Lemiale, V., Robinson, G.K., Ye, F., Ouyang, S., Tang, X., 2015. A scenario-based risk framework for determining consequences of different failure modes of earth dams. Nat. Hazards 75, 1489–1530. https://doi.org/10.1007/s11069-014-1379-x

Clément, R., Descloitres, M., Günther, T., Ribolzi, O., Legchenko, A., 2009. Influence of shallow infiltration on time-lapse ERT: Experience of advanced interpretation. Comptes Rendus - Geosci. 341, 886–898. https://doi.org/10.1016/j.crte.2009.07.005

Constable, S.C., Parker, R.L., Constable, C.G., 1987. Occam's inversion: A practical algorithm for generating smooth models from electromagnetic sounding data. Geophysics 52, 289–300. https://doi.org/10.1190/1.1442303

Dahlin, T., Zhou, B., 2004. A numerical comparison of 2D resistivity imaging with 10 electrode arrays. Geophys. Prospect. 52, 379–398. https://doi.org/10.1111/j.1365-2478.2004.00423.x

De Groot-Hedlin, C., Constable, S., 1990. Occam's inversion to generate smooth, two-dimensional models from magnetotelluric data. Geophysics 55, 1613–1624. https://doi.org/10.1190/1.1442813

Donohue, S., Gavin, K., Tolooiyan, A., 2011. Geophysical and geotechnical assessment of a railway embankment failure. Near Surf. Geophys. 9, 33–44. https://doi.org/10.3997/1873-0604.2010040

Fargier, Y., Palma Lopes, S., Fauchard, C., François, D., Côte, P., 2014. DC-Electrical Resistivity Imaging for embankment dike investigation: A 3D extended normalisation approach. J. Appl. Geophys. 103, 245–256. https://doi.org/10.1016/j.jappgeo.2014.02.007

Fauchard, C., Mériaux, P., 2007. Geophysical and geotechnical methods for diagnosing flood protection dikes, Guide for Implementation and Interpretation, Quae, 124p. ed.

Fell, R., Fry, J.-J., 2007. The state of the art of assessing the likelihood of internal erosion of embankment dams, water retaining structures and their foundations, in: Internal Erosion of Dams and Their Foundations. Taylor & Francis / Balkerna, pp. 9–32.

Glendinning, S., Hughes, P., Helm, P., Chambers, J., Mendes, J., Gunn, D., Wilkinson, P., Uhlemann, S., 2015. Construction, management and maintenance of embankments used for road and rail infrastructure: implications of weather induced pore water pressures. Acta Geotech. 799–816. https://doi.org/10.1007/s11440-014-0324-1

Goyal, V.C., Gupta, P.K., Seth, S.M., Singh, V.N., 1996. Estimation of temporal changes in soil moisture using resistivity method. Hydrol. Process. 10, 1147–1154. https://doi.org/10.1002/(SICI)1099-1085(199609)10:9<1147::AID-HYP366>3.0.CO;2-S

Gupta, S.C., Hanks, R.J., 1972. Influence of Water Content on Electrical Conductivity of the Soil. Soil Sci. Soc. Am. J. 36, 855–857. https://doi.org/10.2136/sssaj1972.03615995003600060011x

Gupta, P.K., Niwas, S., Gaur, V.K., 1997. Straightforward inversion of vertical electrical sounding data. Geophysics 62, 775–785. https://doi.org/10.1190/1.1444187

Hayley, K., Bentley, L.R., Gharibi, M., Nightingale, M., 2007. Low temperature dependence of electrical resistivity: Implications for near surface geophysical monitoring. Geophys. Res. Lett. 34, 1–5. https://doi.org/10.1029/2007GL031124

Hayley, K., Bentley, L.R., Pidlisecky, A., 2010. Compensating for temperature variations in time-lapse electrical resistivity difference imaging. Geophysics 75, WA51. https://doi.org/10.1190/1.3478208

Huang, W.-C., Weng, M.-C., Chen, R.-K., 2014. Levee failure mechanisms during the extreme rainfall event: a case study in Southern Taiwan. Nat. Hazards 70, 1287–1307. https://doi.org/10.1007/s11069-013-0874-9

Jackson, P.D., Northmore, K.J., Meldrum, P.I., Gunn, D.A., Hallam, J.R., Wambura, J., Wangusi, B., Ogutu, G., 2002. Non-invasive moisture monitoring within an earth embankment - A precursor to failure. NDT E Int. 35, 107–115. https://doi.org/10.1016/S0963-8695(01)00030-5

Janik, G., Dawid, M., Walczak, A., Słowińska-Osypiuk, J., Skierucha, W., Wilczek, A., Daniel, A., 2017. Application of the TDR technique for the detection of changes in the internal structure of an earthen flood levee. J. Geophys. Eng. 14, 292. https://doi.org/10.1088/1742-2140/14/2/292

Jodry, C., Palma Lopes, S., Fargier, Y., Côte, P., Sanchez, M., 2017. A cost-effective 3D Electrical Resistivity Imaging approach applied to Dike investigation. Near Surf. Geophys. 15, 27–41. https://doi.org/10.3997/1873-0604.2016036

Johansson, S., Dahlin, T., 1996. Seepage monitoring in an earth embankment dam by repeated resistivity measurements. Eur. J. Environ. Eng. Geophys. 1, 229–247.

Kappelmeyer, O., 1957. The use of near surface temperature measurements for discovering anomalies due to causes at depths. Geophys. Prospect. 5, 239–258. https://doi.org/10.1111/j.1365-2478.1957.tb01431.x

Karaoulis, M., Tsourlos, P., Kim, J.H., Revill, A., 2014. 4D time-lapse ERT inversion: Introducing combined time and space constraints. Near Surf. Geophys. 12, 25–34. https://doi.org/10.3997/1873-0604.2013004

Keller, G.V., Frischknecht, F.C., 1966. Electrical methods in geophysical prospecting. Pergamon Press, 519 p.

Kim, J.-H., Yi, M.-J., Song, Y., Seol, S.J., Kim, K.-S., 2007. Application of geophysical methods to the safety analysis of an earth dam. J. Environ. Eng. Geophys. 12, 221–235. https://doi.org/10.2113/JEEG12.2.221

Kuras, O., Pritchard, J.D., Meldrum, P.I., Chambers, J.E., Wilkinson, P.B., Ogilvy, R.D., Wealthall, G.P., 2009. Monitoring hydraulic processes with automated time-lapse electrical resistivity tomography (ALERT). Comptes Rendus - Geosci. 341, 868–885. https://doi.org/10.1016/j.crte.2009.07.010

Lin, C.P., Hung, Y.C., Yu, Z.H., Wu, P.L., 2013. Investigation of abnormal seepages in an earth dam using resistivity tomography. J. Geoengin. 8, 61–70. https://doi.org/10.6310/jog.2013.8(2).4

Lin, C.-P., Hung, Y.-C., Wu, P.-L., Yu, Z.-H., 2014. Performance of 2-D ERT in Investigation of Abnormal Seepage: A Case Study at the Hsin-Shan Earth Dam in Taiwan. J. Environ. Eng. Geophys. 19, 101–112. https://doi.org/10.2113/JEEG19.2.101

Loke, M.H., Barker, R.D., 1996. Rapid least-squares inversion of apparent resistivity pseudosections by a quasi-Newton method. Geophys. Prospect. 44, 131–152. https://doi.org/10.1111/j.1365-2478.1996.tb00142.x

Loke, M.H., Acworth, I., Dahlin, T., 2003. A comparison of smooth and blocky inversion methods in 2D electrical imaging surveys. Explor. Geophys. 34, 182–187. https://doi.org/10.1071/EG03182

Loke, M.H., Chambers, J.E., Rucker, D.F., Kuras, O., Wilkinson, P.B., 2013. Recent developments in the direct-current geoelectrical imaging method. J. Appl. Geophys. 95, 135–156. https://doi.org/10.1016/j.jappgeo.2013.02.017

Loperte, A., Soldovieri, F., Palombo, A., Santini, F., Lapenna, V., 2016. An integrated geophysical approach for water infiltration detection and characterization at Monte Cotugno rock-fill dam (southern Italy). Eng. Geol. 211, 162–170. https://doi.org/10.1016/j.enggeo.2016.07.005

Marescot, L., Rigobert, S., Palma Lopes, S., Lagabrielle, R., Chapellier, D., 2006. A general approach for DC apparent resistivity evaluation on arbitrarily shaped 3D structures. J. Appl. Geophys. 60, 55–67. https://doi.org/10.1016/j.jappgeo.2005.12.003

Menke, W., 1984. Geophysical data analysis: discrete inverse theory. Academic Press Inc., 272p.

Miller, C.R., Routh, P.S., Brosten, T.R., McNamara, J.P., 2008. Application of time-lapse ERT imaging to watershed characterization. Geophysics 73, G7–G17. https://doi.org/10.1190/1.2907156

Musy, A., Soutter, M., 1991. Chap. 5 - Thermique du sol, 5.4 Régime thermique, 5.4.1 Cycles de variations thermiques, in: Physique du sol. Presses polytechniques et universitaires Romandes (Ed.), Physique Du Sol. pp. 163–166.

Niederleithinger, E., Weller, A., Lewis, R., 2012. Evaluation of geophysical techniques for dike inspection. J. Environ. Eng. Geophys. 17, 185–195. https://doi.org/10.2113/JEEG17.4.185

Ogilvy, R.D., Meldrum, P.I., Kuras, O., Wilkinson, P.B., Chambers, J.E., Sen, M., Pulido-Bosch, A., Gisbert, J., Jorreto, S., Frances, I., Tsourlos, P.I., 2009. Automated monitoring of coastal aquifers with electrical resistivity tomography. Near Surf. Geophys. 7, 367–375. https://doi.org/10.3997/1873-0604.2009027

Panthulu, T. V, Krishnaiah, C., Shirke, J.M., 2001. Detection of seepage paths in earth dams using self-potential and electrical resistivity methods. Eng. Geol. 59, 281–295. https://doi.org/10.1016/S0013-7952(00)00082-X

Pellicer, X.M., Zarroca, M., Gibson, P., 2012. Time-lapse resistivity analysis of Quaternary sediments in the Midlands of Ireland. J. Appl. Geophys. 82, 46–58. https://doi.org/10.1016/j.jappgeo.2012.02.009

Perri, M.T., Boaga, J., Bersan, S., Cassiani, G., Cola, S., Deiana, R., Simonini, P., Patti, S., 2014. River embankment characterization: The joint use of geophysical and geotechnical techniques. J. Appl. Geophys. 110, 5–22. https://doi.org/10.1016/j.jappgeo.2014.08.012

Rhoades, J.D., Raats, P.A.C., Prather, R.J., 1976. Effects of Liquid-phase Electrical Conductivity, Water Content, and Surface Conductivity on Bulk Soil Electrical Conductivity. Soil Sci. Soc. Am. J. 40, 651. https://doi.org/10.2136/sssaj1976.03615995004000050017x

Rings, J., Scheuermann, A., Preko, K., Hauck, C., 2008. Soil water content monitoring on a dike model using electrical resistivity tomography. Near Surf. Geophys. 6, 123–132. https://doi.org/10.3997/1873-0604.2007038

Royet, P., Palma Lopes, S.S., Fauchard, C., Mériaux, P., Auriau, L., 2013. FloodproBE Project report WP 3: Reliability of Urban Flood Defences. D3.2: Rapid and cost-effective dike condition assessment methods: geophysics and remote sensing. 136 p.

Rücker, C., Günther, T., Spitzer, K., 2006. Three-dimensional modelling and inversion of dc resistivity data incorporating topography - I. Modelling. Geophys. J. Int. 166, 495–505. https://doi.org/10.1111/j.1365-246X.2006.03010.x

Samouëlian, A., Cousin, I., Tabbagh, A., Bruand, A., Richard, G., 2005. Electrical resistivity survey in soil science: A review. Soil Tillage Res. 83, 173–193. https://doi.org/10.1016/j.still.2004.10.004

Sentenac, P., Benes, V., Budinsky, V., Keenan, H., Baron, R., 2017. Post flooding damage assessment of earth dams and historical reservoirs using non-invasive geophysical techniques. J. Appl. Geophys. 146, 138–148. https://doi.org/10.1016/j.jappgeo.2017.09.006

Sjödahl, P., Dahlin, T., Johansson, S., 2005. Using resistivity measurements for dam safety evaluation at Enemossen tailings dam in southern Sweden. Environ. Geol. 49, 267–273. https://doi.org/10.1007/s00254-005-0084-1

Sjödahl, P., Dahlin, T., Johansson, S., Loke, M.H., 2008. Resistivity monitoring for leakage and internal erosion detection at Hällby embankment dam. J. Appl. Geophys. 65, 155–164. https://doi.org/10.1016/j.jappgeo.2008.07.003

Sjödahl, P., Dahlin, T., Johansson, S., 2009. Embankment dam seepage evaluation from resistivity monitoring data. Near Surf. Geophys. 7, 463–474. https://doi.org/10.3997/1873-0604.2009023

Sjödahl, P., Dahlin, T., Johansson, S., 2010. Using the resistivity method for leakage detection in a blind test at the Røssvatn embankment dam test facility in Norway. Bull. Eng. Geol. Environ. 69, 643–658. https://doi.org/10.1007/s10064-010-0314-y

Telford, W.M., Geldart, L.P., Sheriff, R.E., 1990. Applied Geophysics, Second Edition. Cambridge University Press. 744p. https://doi.org/10.1017/CBO9781139167932

Utili, S., Castellanza, R., Galli, A., Sentenac, P., 2015. Novel Approach for Health Monitoring of Earthen Embankments. J. Geotech. Geoenvironmental Eng. 141, 04014111.1-04014111.19. https://doi.org/10.1061/(ASCE)GT.1943-5606.0001215.

Weller, A., Canh, T., Breede, K., Vu, N.T., 2006. Multi-electrode measurements at Thai Binh dikes (Vietnam). Near Surf. Geophys. 4, 135–143. https://doi.org/10.3997/1873-0604.2005039

Weller, A., Lewis, R., Canh, T., Moller, M., Scholz, B., 2014. Geotechnical and Geophysical Long-term Monitoring at a Levee of Red River in Vietnam. J. Environ. Eng. Geophys. 19, 183–192. https://doi.org/10.2113/JEEG19.3.183

Wiwattanachang, N., Giao, P.H., 2011. Monitoring crack development in fiber concrete beam by using electrical resistivity imaging. J. Appl. Geophys. 75, 294–304. https://doi.org/10.1016/j.jappgeo.2011.06.009

Highlights for the following paper

"2D-ERT monitoring of soil moisture seasonal behaviour in a river levee: A case study".

- Installation of permanent electrodes allows high quality long-term apparent resistivity time series.
- Temperature compensation yields consistent percentage resistivity changes in the levee body.
- Seasonal monitoring of an old stretch of levee by electrical resistivity imaging proves efficient.
- Levee soil moisture behaviour is clearly influenced by rainfall and water table and river levels.